Molybdenum(0) Fischer ethoxycarbene complexes:

Synthesis, X-ray crystal structures and DFT study

Armand Jansen van Rensburg,[a] *Marilé Landman,*[a]* *Petrus H. van Rooyen,*[a] *Marrigje M. Conradie*[b] *and Jeanet Conradie*[b]*

[a] Department of Chemistry, University of Pretoria, Private Bag X20, Hatfield, 0028, South Africa. Tel: 27-12-4202527, Fax: 27-12-4204687

[b] Department of Chemistry, University of the Free State, PO Box 339, Bloemfontein, 9300, South Africa. Tel: 27-51-4012194, Fax: 27-51-4017295

Contact author details:

Name: Jeanet Conradie, Tel: ++27-51-4012194, Fax: ++27-51-4017295, email: conradj@ufs.ac.za

Name: Marilé Landman Tel: ++27-12-4202527, Fax: ++27-12-4204687, email: marile.landman@up.ac.za

SYNOPSIS TOC

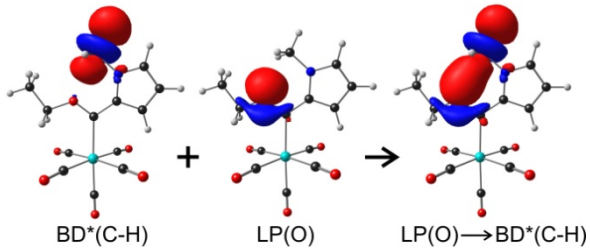

Abstract

The synthesis and structural investigations are presented of molybdenum(0) Fischer carbene complexes with general formula [L(CO)$_4$MoC(OEt)(Ar)] with L = CO, PPh$_3$, AsPh$_3$ and Ar = 2-thienyl, 2-furyl, 2-(N-methyl)pyrrolyl, 2,2'-bithienyl. The X-ray crystal structures, along with NMR and IR spectroscopy, revealed a *cis*-orientation of the carbene and pnictogen ligands (PPh$_3$ or AsPh$_3$) for all the substituted complexes. A density functional theory study of all possible conformers indicated, in agreement with experimental results, that the *cis*-isomers (PPh$_3$ or AsPh$_3$ *cis* relative to the carbene ligand) are more stable than the corresponding *trans*-isomers, and that most stable conformers have the aryl group *syn* to the ethoxy group for Ar = 2-thienyl, 2-(N-methyl)pyrrolyl, 2,2'-bithienyl and *anti* to the ethoxygroup for Ar = 2-furyl.

Keywords
Fischer carbene; Molybdenum; Triphenylphosphine; Triphenylarsine; conformations; DFT

1 Introduction

Fischer carbene complexes of group VIB and VIIB metal carbonyl complexes are abundant. For group VIB metals, chromium(0) and tungsten(0) Fischer carbene complexes far outnumber Fischer carbene complexes of molybdenum(0). This is due to the higher stability of the former complexes [1-3], making them the preferential choice for industrial and academic applications. Fischer and his co-workers reported that the incorporation of a pnictogen-type ligand (ER_3, E = P, As, Sb and R = alkyl, aryl) into the coordination sphere of a Fischer carbene complex resulted in air-tolerant complexes [4-6]. Fischer and Aumann reported the synthesis of complexes *cis*-[$(EPh_3)(CO)_4WC(OMe)(R)$] with E = P, As, Sb and R = Me or Ph, as well as *cis*-[$(PPh_3)(CO)_4MC(OMe)(Me)$] with M = Cr and M = Mo [4]. Fischer and Fischer reported a series of *cis*- and *trans*-substituted Fischer carbene complexes of Cr(0) and W(0) using phosphine (PR_3) ligands [5], while the work of Fischer and Richter focused on carbonyl substitution reactions of Fischer alkoxycarbene complexes of Cr(0) with arsines (AsR_3) and stibines (SbR_3) [6]. Various phosphine-type ligands have been used as ancillary ligands in Mo(0) Fischer carbene complexes [4,7,8]; however, no arsine-substituted Fischer carbene complexes of Mo(0) have been reported to date.

Fischer carbene complexes play an important role in organic transformations and template reactions [9-11]. The use of pnictogen ligands [4-6] in Fischer carbene complexes of Mo(0) may augment the stability of the complex without loss of reactivity. The reactivity of a compound is determined by its electronic and steric features. Understanding these properties is valuable in the production of compounds with industrial and academic applicability.

The synthesis and structural investigations of Fischer carbene complexes of the type $[(CO)_5MoC(Y)(C_4H_3O)]$, $[(PPh_3)(CO)_4MoC(Y)(C_4H_3O)]$, and $[(dppe)(CO)_3MoC(Y)(C_4H_3O)]$ (dppe = 1,2-bis(diphenylphosphino)ethane) for Y = OEt, NH_2, NHCy were recently reported by our group [12,13]. Furthermore, we also reported the synthesis and structural examination of arsine-substituted Fischer carbene complexes of the type *cis*-[$(AsPh_3)(CO)_4WC(OEt)(Ar)$] for Ar = 2-thienyl, 2-furyl, 2-(N-methyl)pyrrolyl, and

2,2’-bithienyl [14]. Based on the success of the above-mentioned studies, and the lack of similar information for Mo(0) Fischer carbene complexes, the synthesis, structural investigation, and theoretical examination of twelve Mo(0) Fischer carbene complexes are reported here. Eight of the complexes are novel and four are known: $[(CO)_5MoC(OEt)(Ar)]$, with Ar = 2-thienyl (**1)** [15], 2-furyl (**2)** [12], 2-(N-methyl)pyrrolyl (**3**), 2,2'-bithienyl **(4)**; $[(PPh_3)(CO)_4MoC(OEt)(Ar)]$, with Ar = 2-thienyl **(5)** [12], 2-furyl (**6)** [12], 2-(N-methyl)pyrrolyl (**7)**, 2,2'-bithienyl (**8**), and $[(AsPh_3)(CO)_4MoC(OEt)(Ar)]$, with Ar = 2-thienyl (**9**), 2-furyl (**10**), 2-(N-methyl)pyrrolyl (**11**), 2,2'-bithienyl (**12**) (Figure 1).

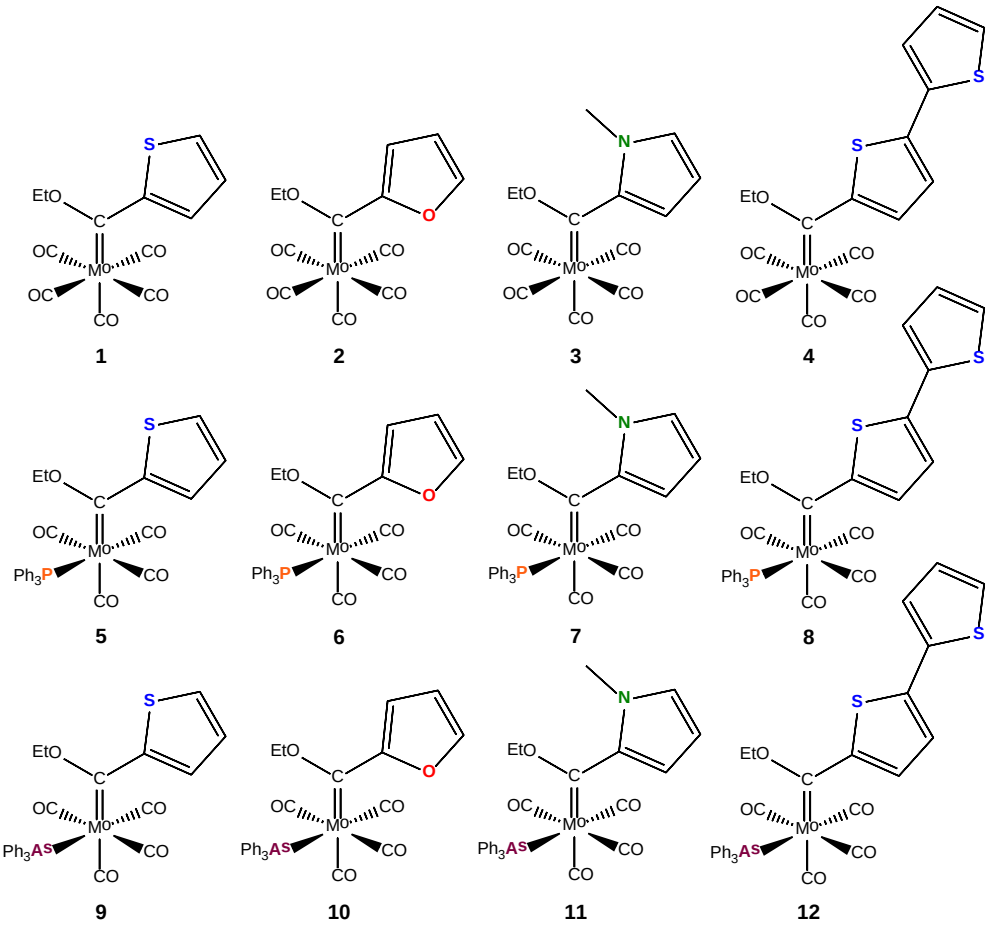

Figure 1. Molybdenum(0) Fischer carbene complexes of this study

2 Experimental

2.1 General

All reactions were performed under inert argon atmospheres using standard Schlenk techniques. Tetrahydrofuran (THF) and diethyl ether were dried using sodium benzophenone ketyl, while dichloromethane (DCM) and hexane were dried using phosphorus pentoxide and metallic sodium, respectively. Analytical grade ethyl acetate was used as purchased. All other solvents were freshly distilled under inert nitrogen or argon atmospheres prior to use. Column chromatography was carried out under inert argon or nitrogen atmospheres at either ambient temperatures or -40 ^{o}C. Silica gel (particle size 0.063 - 0.200 mm) was used as the stationary phase. Percentage yields were calculated relative to the limiting reagent. Crystallization was performed either by vapour diffusion or by slow solvent evaporation, using hexane, DCM, ethyl acetate, and/or diethyl ether as crystallization solvents. Commercial thiophene [16], N-methylpyrrole [17], and N,N,N',N'-tetramethylethylenediamine (TMEDA) [17] were purified using literature procedures. Triethyloxonium tetrafluoroborate was prepared according to the literature method [18]. The reagents molybdenum(0) hexacarbonyl, n-butyllithium (1.6 mol·dm^{-3} in hexane), furan, 2,2'-bithiophene, triphenylphosphine, and triphenylarsine were used as purchased. Nuclear magnetic resonance (NMR) spectra were recorded on a Bruker ARX-300 spectrometer in $CDCl_3$ using the solvent residual peak as the internal reference. ^{1}H, ^{31}P, and ^{13}C NMR spectra were recorded at 300.1, 75.5, and 81 MHz, respectively. Refer to Figure 3 - Figure 10 for the atomic numbering schemes. Infrared (IR) spectra were recorded on a Perkin Elmer Spectrum RXI FT-IR spectrophotometer as potassium bromide pellets, and only the vibration bands in the carbonyl-stretching region (1500 - 2200 cm^{-1}) are reported. Mass spectra were recorded on a SYNAPT G2 HDMS instrument, using electrospray ionization as the ion source and a time-of-flight mass analyzer. A sampling time of 3 minutes was used, with the direct infusion inlet method.

2.2 Synthesis

The synthesis and purification of the known complexes **1** [15] and **2** [12] were carried out according to the literature methods while known complexes **5** [12] and **6** [12] were synthesized with slight modification to the literature method.

*2.2.1 [(CO)$_5$MoC(OEt)(C$_4$H$_3$NMe)] (**3**)*

Freshly distilled N-methylpyrrole (0.44 mℓ, 5.0 mmol) and TMEDA (0.74 mℓ, 5.0 mmol) were dissolved in hexane (40 mℓ), and n-butyllithium (3.34 mℓ, 5.0 mmol, 1.6 mol·dm^{-3} in hexane) was added. The mixture was refluxed for 9 hours under stringent inert conditions, resulting in a milky white solution. Heating was ceased and the solvent was removed under reduced pressure. The resulting white residue was cooled to -78 °C and [Mo(CO)$_6$] (1.32 g, 50 mmol) in THF (40 mℓ) was added in one portion. The mixture was stirred at -78 °C for 30 minutes, followed by stirring at ambient temperature for 60 minutes, yielding a brown-orange solution. The solvent was removed under reduced pressure, and the resulting brown residue was dissolved in DCM (30 mℓ) and cooled to -20 °C. Triethyloxonium tetrafluoroborate (1.4 g, 7.36 mmol) in DCM (10 mℓ) was added to the cooled solution. The mixture was stirred at -20 °C for 30 minutes, followed by stirring at ambient temperature for 30 minutes, resulting in a brown-orange solution. The solvent was removed and the resulting residue was purified using a 25 cm silica gel column at ambient temperature. Hexane-DCM gradient elution yielded **3** as a yellow-orange powder (0.73g, 1.96 mmol, 39 %) after solvent removal. ^{1}H-NMR (CDCl$_3$, ppm) δ 7.74 (dd, 1H, J_{H-H} = 4.5 Hz, 1.7 Hz, H8), 6.90 (s(br), 1H, H10), 6.32 (dd, 1H, J_{H-H} = 4.4 Hz, 2.4 Hz, H9), 5.02 (q, 2H, J_{H-H} = 7.1 Hz, H11), 3.81 (s(br), 3H, H13), 1.66 (t, 3H, J_{H-H} = 7.1 Hz, H12); ^{13}C{^{1}H}-NMR (CDCl$_3$, ppm) δ 293.3 (C6), 213.1 (C1), 206.8 (C2, C3, C4, and C5), 144.5 (C7), 136.1 (C8), 134.8 (C10), 111.1 (C9), 77.2 (C11), 40.6 (C13), 15.5 (C12); IR (KBr, *ν*(CO)/cm^{-1}) 2063, s (A_1^1), 1976, vs (B), 1912, vs (A_1^2), 1950, m (E); MS (m/z): Calc. 374.96 [M]$^+$, Exp. 376.0 [M+H]$^+$.

*2.2.2 [(CO)$_5$MoC(OEt)(C$_8$H$_5$S$_2$)] (**4**)*

2,2'-Bithiophene (0.83 g, 5.0 mmol) was dissolved in THF (40 mℓ), and cooled to -40 °C. A solution of n-butyllithium (3.34 mℓ, 5.0 mmol, 1.6 mol·dm^{-3} in hexane) was added to the cooled solution, and the mixture was stirred at -40 °C for 30 minutes, followed by stirring at ambient temperature for 30 minutes. The solution was then cooled to -78 °C, and [Mo(CO)$_6$] (1.32 g, 5.0 mmol) was added in one portion. The mixture was stirred at -78 °C for 30 minutes, followed by stirring at ambient temperature for 60 minutes, yielding a brown solution. The solvent was removed under reduced pressure, yielding a brown residue. The residue was dissolved in DCM (30 mℓ) and cooled to -20 °C. Triethyloxonium tetrafluoroborate (1.4 g, 7.36 mmol) in DCM (10 mℓ) was added to the cooled solution. The mixture was stirred at -20 °C for 30 minutes, followed by stirring at ambient temperature for

30 minutes, resulting in a brown-red solution. The solvent was removed under reduced pressure, and the resulting residue was purified using a 25 cm silica gel column at ambient temperature. Hexane elution yielded **4** as a crimson powder (1.16 g, 2.53 mmol, 51%). ^{1}H-NMR ($CDCl_3$, ppm) δ 8.16 (d, 1H, J_{H-H} = 4.3 Hz, H8), 7.44 (dd, 1H, J_{H-H} = 3.7 Hz, 1.1 Hz, H16), 7.42 (dd, 1H, J_{H-H} = 5.1 Hz, 3.6 Hz, H14), 7.33 (d, 1H, J_{H-H} = 4.3 Hz, H9), 7.11 (dd, 1H, J_{H-H} = 5.1 Hz, 3.7 Hz, H15), 5.07 (q, 2H, J_{H-H} = 7.1 Hz, H11), 1.68 (t, 3H, J_{H-H} = 7.1 Hz, H12); ^{13}C{^{1}H}-NMR ($CDCl_3$, ppm) δ 302.8 (C6), 212.9 (C1), 206.2 (C2, C3, C4, and C5), 153.0 (C7), 148.0 (C10), 143.6 (C8), 136.3 (C13), 128.5 (C15), 127.7 (C14), 126.4 (C16), 125.2 (C9), 77.2 (C11), 15.1 (C12); IR (KBr, ν(CO)/cm^{-1}) 2060, s (A_1^1), 1972, m (B), 1915, vs (A_1^2), 1948, s (E); MS (m/z): Calc. 459.90 $[M]^+$, Exp. 460.9 $[M+H]^+$.

*2.2.3 cis-[(PPh_3)$(CO)_4$MoC(OEt)(C_4H_3S)] (**5**)* [12]

Complex **1** (0.19 g, 0.5 mmol) and PPh_3 (0.14 g, 0.55 mmol) were dissolved in hexane (40 mℓ), producing a dark red solution. The solution was heated to reflux temperature, and was stirred at this temperature for 2 hours, yielding a red-brown solution. Thin-layer chromatography (TLC) analysis (Hexane-DCM (4:1)) indicated a mixture of unreacted starting materials along with two substitution products: a dark brown compound and a yellow-brown compound. Heating was ceased and the solvent was removed under reduced pressure. The resulting brown residue was purified using a 20 cm silica gel column at -40 °C. Hexane elution yielded unreacted **1** as a red fraction while hexane-DCM gradient elution yielded **5** as a dark brown fraction. After solvent removal, **5** was obtained as a metallic brown powder (0.23 g, 0.38 mmol, 75%). The *trans*-isomer of **5**, *trans*-[(PPh_3)$(CO)_4$MoC(OEt)(C_4H_3S)], was observed as a yellow-brown fraction migrating ahead of **5**. The *trans*-isomer decomposed or isomerized to **5** before elution could occur. ^{1}H-NMR ($CDCl_3$, ppm, see reference [12] for NMR data in C_6D_6) δ 7.87 (d, 1H, J_{H-H} = 4.0 Hz, 1.1 Hz, H8), 7.57 (dd, 1H, J_{H-H} = 5.0 Hz, 1.1 Hz, H10), 7.29 - 7.44 (m, 15H, P**Ph**$_3$), 6.98 (dd, 1H, J_{H-H} = 5.0 Hz, 4.0 Hz, H9), 4.65 (q, 2H, J_{H-H} = 7.0 Hz, H11), 1.21 (t, 3H, J_{H-H} = 7.1 Hz, H12); ^{31}P-NMR ($CDCl_3$, ppm) δ 40.0 (**P**Ph_3); ^{13}C{^{1}H}-NMR ($CDCl_3$, ppm) δ 310.5 (d, J_{P-C} = 7.9Hz, C6), 218.9 (d, J_{P-C} = 8.8 Hz, C1), 216.1 (d, J_{P-C} = 25.3 Hz, C3), 210.2 (d, J_{P-C} = 8.8 Hz, C2 and C4), 156.6 (C7), 140.2 (C10), 135.6 (d, J_{P-C} = 31.8 Hz, C13), 133.2 (d, J_{P-C} = 12.2 Hz, C14), 132.6 (C8), 129.8 (C16), 128.7 (C9), 128.4 (d, J_{P-C} = 9.1 Hz, C15), 77.2 (C11), 14.8 (C12); IR (KBr, ν(CO)/cm^{-1}) 2011, m (A_1^1), 1917, s (A_1^2), 1903, s (B_1), 1884, vs (B_2).

*2.2.4 cis-[(PPh_3)$(CO)_4$MoC(OEt)(C_4H_3O)] (**6**)* [12]

Complex **2** (0.19 g, 0.5 mmol) and PPh_3 (0.14 g, 0.55 mmol) were dissolved in hexane (40 mℓ), producing a red solution. The solution was stirred at refluxing temperature for 2 hours, resulting in a colour change from red to brown. TLC analysis (Hexane-DCM (4:1)) indicated a mixture of unreacted starting materials and substitution products: a red-brown compound and a pale brown compound. Heating was stopped and the solvent was removed under reduced pressure. The resulting brown residue was purified using a 20 cm silica gel column at -40 °C. Unreacted **2** was eluted with hexane as a red fraction, while hexane-DCM gradient elution was used for the elution of **6** as a red-brown fraction. After solvent removal, **6** was obtained as a brown crystalline powder (0.21 g, 0.35 mmol, 71%). The *trans*-isomer of **6**, *trans*-[(PPh_3)$(CO)_4$MoC(OEt)(C_4H_3O)], was observed as a pale brown fraction migrating ahead of **6**. The *trans*-isomer decomposed or isomerized to **6** before elution occurred. ^{1}H-NMR ($CDCl_3$, ppm, see reference [12] for NMR data in CD_2Cl_2) δ 7.32 - 7.42 (m, 15H, P**Ph**$_3$), 7.29 (s(br), 1H, H10), 6.76 (d, 1H, J_{H-H} = 3.6 Hz, H8), 6.35 (dd, 1H, J_{H-H} = 3.6 Hz, 1.7 Hz, H9), 4.80 (q, 2H, J_{H-H} = 7.0 Hz, H11), 1.37 (t, 3H, J_{H-H} = 7.1 Hz, H12); ^{31}P-NMR ($CDCl_3$, ppm) δ 40.4 (**P**Ph_3); ^{13}C{^{1}H}-NMR ($CDCl_3$, ppm) δ 304.5 (d, J_{P-C} = 8.6 Hz, C6), 219.6 (d, J_{P-C} = 8.5 Hz, C1), 216.4 (d, J_{P-C} = 25.2 Hz C3), 210.4 (d, J_{P-C} = 8.6 Hz, C2 and C4), 164.4 (C7), 150.0 (C10), 136.2 (d, J_{P-C} = 31.5 Hz, C13), 133.3 (d, J_{P-C} = 12.4 Hz, C14), 129.5 (C16), 128.2 (d, J_{P-C} = 9.5 Hz, C15), 112.4 (C8), 111.9 (C9), 77.2 (C11), 15.1 (C12).

*2.2.5 cis-[(PPh_3)$(CO)_4$MoC(OEt)(C_4H_3NMe)] (**7**)*

Complex **3** (0.19g, 0.5 mmol) and PPh_3 (0.14 g, 0.55 mmol) were dissolved in hexane (30 mℓ), yielding a yellow-orange solution. The mixture was heated to reflux temperature, and was stirred at this temperature for 2 hours. TLC analysis (hexane-DCM (3:2)) revealed the formation of a two products: a red compound and an orange compound, as well as unreacted starting materials. Heating was ceased and the solvent was removed under reduced pressure. The resulting orange-red residue was purified using a 20 cm silica gel column at -40 °C. Unreacted **3** was eluted with hexane as a yellow fraction, and gradient elution with hexane and DCM yielded **7** as a red powder (0.22 g, 0.36 mmol, 72%). The orange compound observed on TLC was not observed on the column during purification. ^{1}H-NMR ($CDCl_3$, ppm) δ 7.34 - 7.40 (m, 15H, P**Ph**$_3$), 7.30 (dd, 1H, J_{H-H} = 4.5 Hz, 1.6 Hz, H8), 6.71 (t, 1H, J_{H-H} = 2.1 Hz, H10), 6.02 (dd, 1H, J_{H-H} = 4.4 Hz, 2.4 Hz, H9), 4.64 (q, 2H, J_{H-H} = 7.1 Hz, H11), 3.63 (s(br), 3H, H13), 1.24 (t, 3H, J_{H-H} = 7.1 Hz, H12); ^{31}P-NMR ($CDCl_3$, ppm) δ 40.5

(**P**Ph_3); IR (KBr, ν(CO)/cm^{-1}) 2008, s (A_1^1), 1923, s (A_1^2), 1896, vs (B_1), 1882, vs (B_2); MS (m/z): Calc. 609.06 $[M]^+$, Exp. 610.1 $[M+H]^+$.

*2.2.6 cis-[(PPh_3)$(CO)_4$MoC(OEt)($C_8H_5S_2$)] (**8**)*

Complex **4** (0.23 g, 0.5 mmol) and PPh_3 (0.14g, 0.55 mmol) were dissolved in hexane (40 mℓ), resulting in a crimson solution. Heating was initiated, and the crimson solution was stirred at refluxing temperature for 2 hours. After this time elapsed, the solution colour changed from crimson to purple-brown. TLC analysis (hexane-DCM (4:1)) revealed the formation of a purple complex as the major product, a brown compound as the minor product, and unreacted starting materials. Heating was stopped and the solvent was removed under reduced pressure. The resulting purple-brown residue was purified using a 20 cm silica gel column at -40 °C. Hexane was used to elute unreacted **4**, while hexane-DCM gradient elution was used to elute **8** as a purple fraction. After solvent removal, **8** was obtained as a purple crystalline powder (0.24 g, 0.34 mmol, 68%). A brown fraction, migrating ahead of the purple fraction, was observed. This fraction corresponds to *trans*-[(PPh_3)$(CO)_4$MoC(OEt)($C_8H_5S_2$)], which decomposed or isomerized to **8** before elution occurred. ^{1}H-NMR ($CDCl_3$, ppm) δ 7.76 (d, 1H, J_{H-H} = 4.2 Hz, H8), 7.36 - 7.43 (m, 15H, P**Ph**$_3$), 7.35 (s(br), 1H, H14), 7.34 (d, 1H, J_{H-H} = 1.3 Hz, H16), 7.08 (dd, 1H, J_{H-H} = 3.8 Hz, 5.2 Hz, H15), 7.05 (d, 1H, J_{H-H} = 4.3 Hz, H9), 4.67 (q, 2H, J_{H-H} = 7.0 Hz, H11), 1.25 (t, 3H, J_{H-H} = 7.1 Hz, H12); ^{31}P-NMR ($CDCl_3$), δ 40.0 (**P**Ph_3); ^{13}C{^{1}H}-NMR ($CDCl_3$), δ 307.1 (d, J_{P-C} = 7.9 Hz, C6), 219.0 (d, J_{P-C} = 8.6 Hz, C1), 216.2 (d, J_{P-C} = 24.7 Hz, C3), 210.3 (d, J_{P-C} = 8.7 Hz, C2 and C4), 153.9 (C7), 144.6 (C10), 142.0 (C8), 137.0 (C13), 135.6 (d, J_{P-C} = 32.2 Hz, C17), 133.3 (d, J_{P-C} = 12.4 Hz, C18), 129.8 (C20), 128.4 (d, J_{P-C} = 9.6 Hz, C19), 128.3 (C9), 126.6 (C15), 125.5 (C16), 124.7 (C14), 76.3 (d, J_{P-C} = 2.5 Hz, C11), 14.9 (C12); IR (KBr, ν(CO), cm^{-1}) 2013, s (A_1^1), 1923, s (A_1^2), 1898, vs,sh (B_1), 1864, vs (B_2); MS (m/z): Calc. 693.99 $[M]^+$, Exp. 695.0 $[M+H]^+$.

*2.2.7 cis-[($AsPh_3$)$(CO)_4$MoC(OEt)(C_4H_3S)] (**9**)*

Complex **1** (0.19 g, 0.5 mmol) and $AsPh_3$ (0.17 g, 0.55mmol) were dissolved in hexane (40 mℓ), yielding a dark red solution. The solution was heated to reflux temperature and was stirred at this temperature for 2 hours. TLC analysis (hexane-DCM (4:1)) revealed the formation of a dark brown product, along with unreacted starting materials. Heating was ceased and the solvent was removed under reduced pressure. The resulting brown-red residue

was purified on a 20 cm silica gel column at -40 °C. A red fraction was eluted with hexane, which corresponded to unreacted **1,** while a dark brown fraction was eluted, which corresponded to **9**. After solvent removal, **9** was obtained as a dark brown powder (0.25g, 0.38 mmol, 76%). ^{1}H-NMR ($CDCl_3$, ppm) δ 7.97 (dd, J = 4.1 Hz, 1.1 Hz, H8), 7.57 (dd, J = 5.1 Hz, 1.1 Hz, H10), 7.30 - 7.45 (m, 15H, As**Ph**$_3$), 6.97 (dd, J = 5.0 Hz, 4.1 Hz, H9), 4.74 (q, 2H, J = 7.1 Hz, H11), 1.22 (t, 3H, J = 7.1 Hz, H12); ^{13}C{^{1}H}-NMR ($CDCl_3$, ppm) δ 307.0 (C6), 215.1 (C1), 210.0 (C3), 206.1 (C2 and C4), 156.2 (C7), 139.6 (C13), 133.7 (C14), 136.8 (C10), 132.4 (C8), 128.8 (C9), 128.7 (C15), 128.5 (C16), 77.2 (C11), 15.1 (C12), IR (KBr, ν(CO)/cm^{-1}) 2012, s (A_1^1), 1920, s (A_1^2), 1905, s (B_1), 1885, vs (B_2); MS (m/z): Calc. 655.95 $[M]^+$, Exp. 656.9 $[M+H]^+$.

*2.2.8 cis-[(AsPh$_3$)(CO)$_4$MoC(OEt)(C$_4$H$_3$O)] (**10**)*

Complex **2** (0.18 g, 0.5 mmol) and $AsPh_3$ (0.17 g, 0.55mmol) were dissolved in hexane (40 mℓ), yielding a red solution. The solution was refluxed for 2 hours with continuous stirring, producing a maroon-coloured solution. TLC analysis (hexane-DCM (4:1)) indicated the presence of unreacted starting materials, as well as the formation of a brown compound. Heating was stopped and the solvent was removed *in vacuo*. The resulting brown residue was purified on a 20 cm silica gel column at -40 °C. A red fraction, corresponding to **2**, was eluted with hexane, while a brown fraction was eluted with hexane-DCM gradient elution, which corresponded to **10**. After solvent removal, **10** was obtained as a brown powder (0.23 g, 0.36 mmol, 72%). ^{1}H-NMR ($CDCl_3$, ppm) δ 7.29 - 7.44 (m, 15H, As**Ph$_3$**), 7.23 (d, 1H, J_{H-H} = 1.5 Hz, H10), 6.73 (d, 1H, J_{H-H} = 3.5 Hz, H8), 6.30 (dd, 1H, J_{H-H} = 3.6 Hz, 1.7 Hz, H9), 4.93 (q, 2H, J_{H-H} = 7.1 Hz, H11), 1.43 (t, 3H, J_{H-H} = 7.1 Hz, H12); ^{13}C{^{1}H}-NMR ($CDCl_3$, ppm) δ 305.3 (C6), 213.5 (C1), 210,2 (C3), 206.1 (C2 and C4), 164.4 (C7), 148.3 (C10), 139.6 (C13), 133.7 (C14), 128.7 (C15), 128.5 (C16), 113.2 (C8), 111.1 (C9), 77.2 (C11), 15.2 (C12); IR (KBr, ν(CO)/cm^{-1}) 2016, s (A_1^1), 1926, s (A_1^2), 1876, s (B_1), 1863, s (B_2); MS (m/z): Calc. 639.98 $[M]^+$, Exp. 640.9 $[M+H]^+$.

*2.2.9 cis-[(AsPh$_3$)(CO)$_4$MoC(OEt)(C$_4$H$_3$NMe)] (**11**)*

Complex **3** (0.19 g, 0.5 mmol) and $AsPh_3$ (0.17 g, 0.55mmol) were dissolved in hexane (40 mℓ), yielding an orange solution. The solution was heated to reflux temperature, and was stirred at this temperature for 2 hours. TLC analysis (hexane-DCM (3:2)) revealed the formation of a red product. Heating was ceased and the solvent was removed under reduced

pressure. The resulting red residue was purified on a 20 cm silica gel column at -40 °C, using hexane-DCM gradient elution. An orange fraction was eluted with hexane, which corresponded to **3**. As elution continued, a red fraction was observed, but converted to an orange fraction before isolation could be achieved. Spectroscopic characterization of this fraction matched that of the starting material. Washing the red residue with cold hexane (-10 °C, 4 × 20 mℓ) instead of purification by cold column chromatography yielded an orange-red residue. Characterization of this residue by means of IR spectroscopy and mass spectrometry was possible, but crystallization and NMR spectroscopy resulted in rapid, total decomposition. IR (KBr, ν(CO)/cm^{-1}) 2008, m (A_1^1), 1927, s (A_1^2), 1903, s (B_1), 1867, m (B_2); MS (m/z): Calc. 653.01 $[M]^+$, Exp. 654.0 $[M+H]^+$.

*2.2.10 cis-[(AsPh$_3$)(CO)$_4$MoC(OEt)(C$_8$H$_5$S$_2$)] (**12**)*

Complex **4** (0.23 g, 0.5 mmol) and $AsPh_3$ (0.17 g, 0.55mmol) was dissolved in hexane (40 mℓ), yielding a crimson solution. The solution was heated to reflux temperature, and was stirred at this temperature for 2 hours. TLC analysis (hexane-DCM (4:1)) revealed the formation of a purple product, along with unreacted starting material. Heating was ceased and the solvent was removed *in vacuo*. The resulting purple residue was purified on a 20 cm silica gel column at -40 °C. A crimson fraction was eluted with hexane, which corresponded to **4**. A purple fraction was eluted with hexane-DCM gradient elution, which corresponded to **12**. After solvent removal, a purple crystalline powder (0.25g, 0.34 mmol, 68%) was obtained. ^{1}H-NMR ($CDCl_3$, ppm) δ 7.88 (d, 1H, J = 4.3 Hz, H8), 7.34 - 7.46 (m, 15H, As**Ph**$_3$), 7.33 (d, 1H, J = 1.5 Hz, H14), 7.25 (s(br), 1H, H16), 7.06 - 7.07 (m, 1H, H15), 7.03 (d, 1H, J = 4.3 Hz, H9), 4.75 (q, 2H, J = 7.1, H11), 1.26 (t, 3H, J = 7.1 Hz, H12); ^{13}C{^{1}H}-NMR ($CDCl_3$, ppm) δ 307.6 (C6), 215.1 (C1), 209.8 (C3), 205.5 (C2 and C4), 156.2 (C7), 144.1 (C10), 141.5 (C8), 139.6 (C17), 136.3 (C13), 133.7 (C18),129.3 (C15), 128.9 (C16), 128.7 (C19), 128.5 (C20), 128.3 (C9), 128.0 (C14), 77.8 (C11), 14.7 (C12); IR (KBr, ν(CO)/cm^{-1}) 2013, s (A_1^1), 1925, s (A_1^2), 1898, vs (B_1), 1882, s (B_2); MS (m/z): Calc. 737.94 $[M]^+$, Exp. 739.0 $[M+H]^+$.

2.3 X-ray Crystallography

Crystals suitable for single crystal X-ray diffraction were obtained for **3-5**, **7-10**, and **12**. Crystal data were collected at 150 K on a Bruker D8 Venture kappa geometry diffractometer

with duo Iμs sources, a Photon 100 CMOS detector and APEX II [19] control software using Quazar multi-layer optics monochromated, Mo-*K*α radiation by means of a combination of ϕ and ω scans. Data reduction was performed using SAINT+ [19] and the intensities were corrected for absorption using SADABS [19]. The structures were solved by intrinsic phasing using SHELXTS [20] and refined by full-matrix least squares using SHELXTL and SHELXL-2014 [20]. In the structure refinement, all hydrogen atoms attached to carbon atoms were added in calculated positions and treated as riding on the atom to which they are attached. All non-hydrogen atoms were refined with anisotropic displacement parameters, all isotropic displacement parameters for hydrogen atoms were calculated as $X \times U_{eq}$ of the atom to which they are attached, X = 1.5 for the methyl hydrogens and 1.2 for all other hydrogens. Crystal data, data collection, structure solution and refinement details are available in each CIF (CCDC deposit numbers 1486743-1486750). ORTEP drawings [21] of the structures (Figure 1) are shown in Figure 3-Figure 10, showing the numbering system used with ADP's at the 50% probability level.

2.4 DFT calculations

Density functional theory (DFT) calculations of this study were performed with the hybrid functional B3LYP [22,23] (20% Hartree-Fock exchange) [24] as implemented in the Gaussian 09 program package [25]. Geometries of the neutral complexes were optimized in gas phase with the triple-ζ basis set 6-311G(d,p) on all atoms except Mo and As, where def2-TZVPP [26] was used. Energies reported are gas phase electronic energies. Natural bonding orbital (NBO) calculations [27-30] were performed on the optimized structures by the NBO 3.1 module [31] in Gaussian 09 at the same level of theory. The B3LYP/6-311G(d,p), def2-TZVPP (Mo, As) functional/basis set combination proved to give good agreement with experiment, both with the X-ray geometry geometry, as well as the lowest energy isomer/conformation of group VI Fischer carbene complexes containing an aryl group at the carbene carbon [14,15,32-34].

3 Results and Discussion

3.1 Synthesis

Two general routes exist for the production of substituted tetracarbonyl Fischer carbene complexes (Figure 2). The first route, outlined in Figure 2(a), entails using a homoleptic metal carbonyl complex in carbene synthesis [1,35,36], followed by ligand substitution [5,6,12,37]. This route can theoretically generate both *cis*- and *trans*-substituted tetracarbonyl complexes as the substitution products [5,6], while the *cis*-isomer is typically obtained in higher yield [37]. Alternatively, a carbonyl ligand of a homoleptic metal carbonyl complex can be replaced by a pnictogen ligand [38,39], and the resulting substituted metal pentacarbonyl complex can then be subjected to carbene synthesis (Figure 2(b)) [4]. This method generates solely the *cis*-substituted tetracarbonyl complex [4], as the pnictogen ligand reduces the electrophilicity of the carbonyl ligand *trans* to itself. The separation of the *cis*- and *trans*-isomers can be achieved by means of column chromatography [6] or crystallization, [40] however, interconversion of the two stereoisomers is possible [13,41]. Carbonyl substitution requires metal-carbonyl bond cleavage, which can be facilitated thermally [38] or photochemically [39]. Thermal methods are preferred over ultraviolet irradiation, as this method generates fewer side-products during carbonyl substitution of a Fischer carbene complex [42].

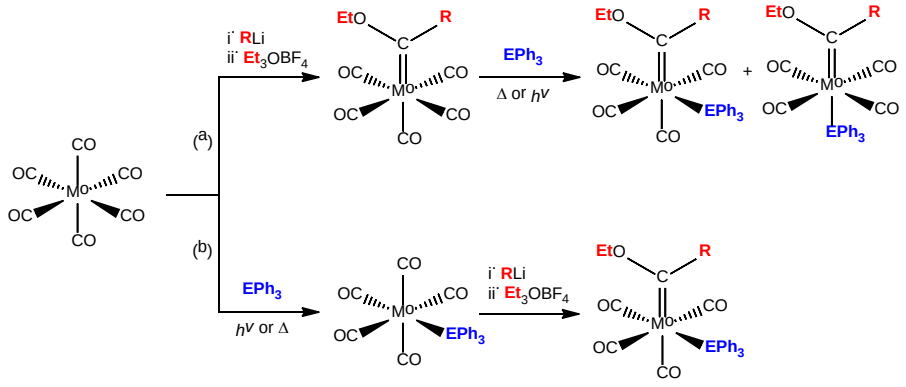

Figure 2. Summary of literature procedures for the synthesis of substituted tetracarbonyl Fischer ethoxycarbene complexes of Mo(0) with R = 2-thienyl, 2-furyl, 2-(N-methyl)pyrrolyl, 2,2'-bithienyl and E = P, As [1,4-6,8,12-15,37-40,42]

The method shown in **Figure 2**(a) was employed in the synthesis of **1** - **12**. In a prior study, the synthesis of *cis*-[($AsPh_3$)$(CO)_4$WC(OEt)(Ar)] (Ar = 2-thienyl, 2-furyl, 2-(N-methyl)pyrrolyl

or 2,2'-bithienyl) could only be achieved using hexane as solvent [14], even though the PPh_3 analogues of these complexes could be prepared using toluene as solvent [12]. Based on this observation, a similar approach was used for the synthesis of **5 - 12**. In accordance with the heightened carbonyl lability of molybdenum(0) complexes as compared to analogous tungsten(0) complexes [43], the reaction time was reduced from 12 hours to 2 hours. Although the *trans*-isomers of the PPh_3 substituted complexes **5 - 8** were observed on TLC as well during column chromatography, none could be isolated. As previously reported [12], the *trans*-substituted Fischer carbene complexes of Mo(0) tend to isomerize or decompose during column chromatography. No *trans*-isomers of the $AsPh_3$-substituted complexes (**9 - 12**) were observed on TLC or during column chromatography. Similarly, the complexes of type *trans*-$[(AsPh_3)(CO)_4WC(OEt)(Ar)]$ (Ar = 2-thienyl, 2-furyl, 2-(N-methyl)pyrrolyl or 2,2'-bithienyl) could also not be isolated [14]. The substituted 2-(N-methyl)pyrrolyl complexes **7** and **11** were less stable than the other six tetracarbonyl complexes of this study. Column chromatography of **11** at -40 ^{o}C resulted in rapid, total decomposition, indicating low *in situ* stability. Similarly, attempted crystallization of **11** was also unsuccessful. The crude product, which is comprised of a mixture of **11** (<10%), unreacted **3** (<45%), and free $AsPh_3$ (>45%), was used for characterization and analyses.

3.2 Characterization

The new complexes **3**, **4**, and **7 - 12** were characterized using ^{1}H, ^{31}P (where applicable), and ^{13}C NMR spectroscopy, IR spectroscopy and electrospray-ionization mass spectrometry. The NMR spectra of **5** and **6** were previously recorded in C_6D_6 and CD_2Cl_2, respectively [12]. In order to correlate the NMR spectral data of these two complexes with that of the other complexes of the study, the NMR spectra of **5** and **6** were re-recorded in $CDCl_3$. The NMR analyses of **7** and **11** were hampered by their low *in situ* stability. The ^{13}C NMR spectrum of **7** could not be obtained, as the complex decomposed during the extended period of the analysis. No NMR spectral data could be obtained for **11**, as this complex decomposed at a much faster rate than **7**.

The ^{1}H NMR spectra of **3 - 12** showed well-resolved carbene ligand protons, except for H15 of **12**, which was observed as a poorly-resolved multiplet. This is not uncommon for Fischer carbene complexes of 2,2'-bithiophene [14,44], and results from proton-proton coupling

occurring between the protons of the 2,2'-bithienyl moiety, and peak overlap on the ^{1}H-NMR spectrum. Poorly-resolved multiplets were also observed for the phenyl-protons of the EPh_3 ligands (E = P, As) in **5 - 10** and **12**, due to extensive peak overlap and proton-proton coupling between the phenyl-protons [12,14]. The carbene ligand protons of the substituted tetracarbonyl complexes **5 - 12** were shifted upfield compared to those of the pentacarbonyl complexes **1 - 4**. Pnictogens and Fischer carbenes are weaker π-acceptor ligands than carbonyls [5]. A tetracarbonyl complex thus contains a metal centre that is richer in electron density than the metal centre of a pentacarbonyl complex [5]. In the former case, the amount of electron density that can be donated to the carbene carbon is greater than in the latter case [37]. The increased extent of π-back-donation from the metal centre to the carbene carbon lessens the extent of electron density withdrawal experienced by the carbene substituents. An upfield shift is observed for the carbene ligand protons of the tetracarbonyl complexes as compared to the corresponding protons in the pentacarbonyl complexes. In comparing the carbene ligand protons of **5 - 8** with that of **9**, **10**, and **12**, no significant difference is observed. The ^{31}P NMR spectra of **5 - 8** showed a peak in the region of 40 ppm. A significant downfield shift is observed from the free (-5.40 ppm) to the coordinated PPh_3 moieties upon metal coordination [45,46]. The ^{13}C NMR spectra of Fischer alkoxycarbene complexes exhibit characteriztic carbene carbon (C6) signals in the region of 280 - 350 ppm. The extremely high downfield shift is due to the electrophilic nature [9] of the electron-deficient carbene carbon. The carbene carbon of the substituted tetracarbonyl complexes (**5**, **6**, **8 - 10** and **12**) were observed at similar or downfield-shifted values than the corresponding parent pentacarbonyl complexes (**1 - 4**) [12,15]. In the case of the pentacarbonyl complexes, two carbonyl carbon signals were observed in the region of 200 - 220 ppm, with a peak height ratio of 1:4. For the tetracarbonyl complexes, three carbonyl carbon signals were observed, with a peak height ratio of 1:1:2. This pattern of carbonyl carbon signals is characteriztic to *cis*-substituted tetracarbonyl complexes [6,14,40]. The chemical shift value of the carbonyl carbon is dependent on the identity of the ligand *trans* to itself [45]. The trend for the chemical shift value of the carbonyl carbon in the linear fragment L-M-CO is as follows: L = carbonyl < arsine < phosphine < carbene [45]. Thus the carbonyl *trans* to the carbene ligand (C1) will be the most downfield shifted, followed by the carbonyl *trans* to the pnictogen (C3), while the carbonyl ligands that are *trans* to one another (C2 and C4) would be the most upfield shifted. The most upfield shifted signal would also represent two carbonyl carbons (C2 and C4), and thus exhibit double the peak height of C1 and C3. The carbonyl carbon

(C3) *trans* to PPh_3 in **5**, **6**, and **8** are shifted downfield by roughly 6 ppm than the carbonyl carbon *trans* to $AsPh_3$ in **9**, **10**, and **12**. This downfield shift is indicative of the increased donor-acceptor strength of PPh_3 over $AsPh_3$ [45]. In the phosphorus-containing complexes, ^{13}C-^{31}P coupling is observed for the carbene, carbonyl, and phenyl carbon atoms [46]. The $^{2}J_{P\text{-}C}$ for the carbonyl carbon *trans* to the PPh_3 ligand is in the range of 25 Hz, while the $^{2}J_{P\text{-}C}$ for the carbon atoms present in the ligands *cis* to the PPh_3 ligand are in the range of 7.9 Hz to 8.8 Hz. This correlates with literature, where the coupling constant is larger for the carbonyl *trans* to the phosphine than for the carbonyl *cis* to the phosphine [45,46]. Furthermore, the phenyl carbons of the PPh_3 ligand also showed ^{13}C-^{31}P coupling, which diminished as the distance between the two coupling nuclei increased. $^{1}J_{P\text{-}C}$ constants of 32 Hz were observed, while $^{2}J_{P\text{-}C}$ constants were found to be roughly 12 Hz, and $^{3}J_{P\text{-}C}$ constants were on average 9.3 Hz. Similar results were obtained by Braterman *et al*. for $[(CO)_5WP(^{n}Bu)_3]$ [45].

The wavenumbers of the carbonyl stretching frequencies on the IR spectra of **5 - 8** are quite similar to those of **9 - 12**. Buchner and Schenk [47] also observed similar carbonyl stretching frequencies for the complexes $[(CO)_5W(EPh_3)]$ with E = P, As, Sb, while the IR spectral data of *cis*-$[(EPh_3)(CO)_4WC(OMe)(Ar)]$ with Ar = Me, E = P, As, and Ar = Ph, E = Sb reported by Fischer and Aumann [4] are similar to that of **5 - 12**. No significant trend is observed for the carbonyl stretching frequencies of **5 - 12**. The donor-acceptor strengths of PPh_3 and $AsPh_3$ in *cis*-$[(EPh_3)(CO)_4MoC(OEt)(Ar)]$ may be too similar to be distinguished by IR spectroscopy. A similar conclusion was drawn by Abel *et al.* [48] in their IR spectral analyses of $[(CO)_3Mo(EPh_3)_3]$ with E = P, As, Sb, where they suggested that the donor-acceptor properties of phosphorous, arsenic, and antimony were remarkably similar.

3.3 X-ray Crystallography

Crystals suitable for single-crystal X-ray diffraction of **5**, **7 - 9** and **12** were obtained by vapour diffusion methods, using hexane and dichloromethane (1:1) solutions, while a diethyl ether-hexane (1:1) mixture was used for the crystallization of **10**. Crystals of **3** were obtained from ethyl acetate-hexane (1:2) solutions, while **4** was crystallized from a hexane solution by slow solvent evaporation. The X-ray crystal structures of **1** [15], **2** [13] and **6** [12] have been reported previously. The molecular structures of **3 - 5**, **7 - 10** and **12** are shown in **Figure 3 - Figure 10**. Selected bond lengths, bond angles, and torsion angles of these complexes are

given in **Table 1** and **Table 2.** Crystal data for all crystal structures determined are given in the electronic supplementary information (ESI), while the details of the data collection and refinement for all eight crystallographic structures are given in the files deposited (CIF).

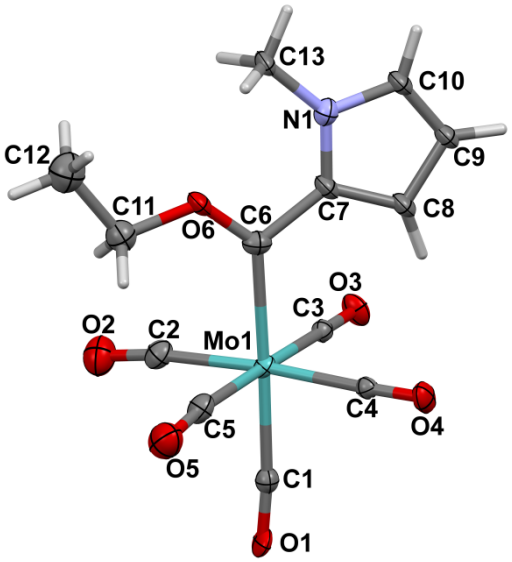

Figure 3. A perspective view of the molecular structure of **3**, showing the atom numbering scheme. Atomic displacement parameters (ADPs) are shown at the 50% probability level.

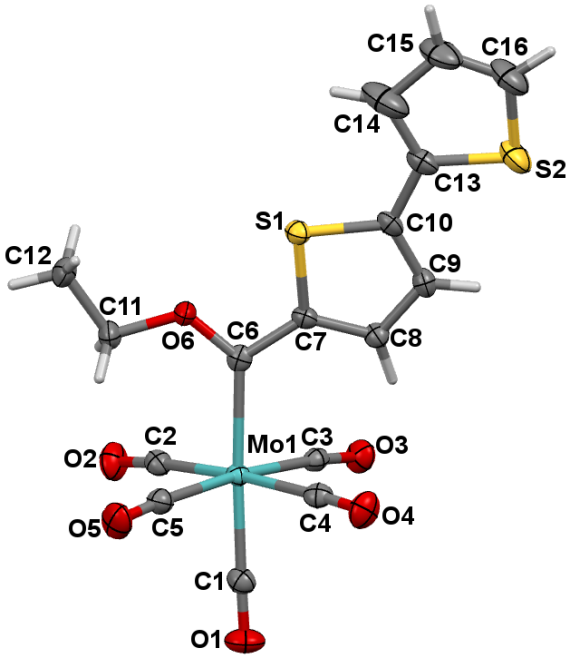

Figure 4. A perspective view of the molecular structure of **4**, showing the atom numbering scheme. Atomic displacement parameters (ADPs) are shown at the 50% probability level.

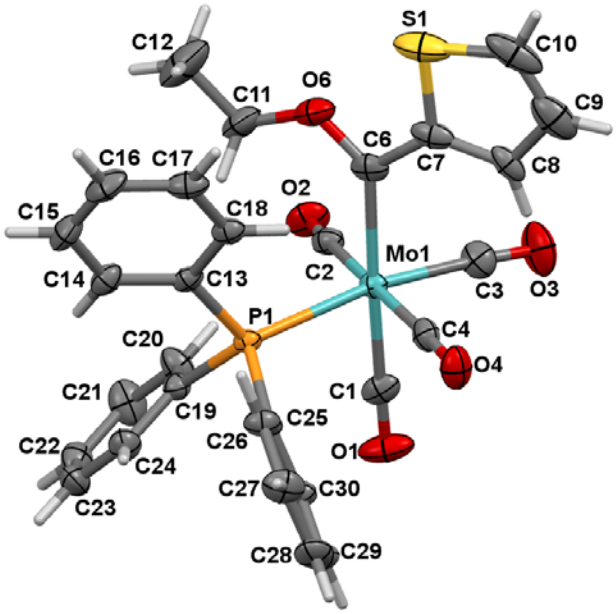

Figure 5. A perspective view of the molecular structure of **5**, showing the atom numbering scheme. Atomic displacement parameters (ADPs) are shown at the 50% probability level.

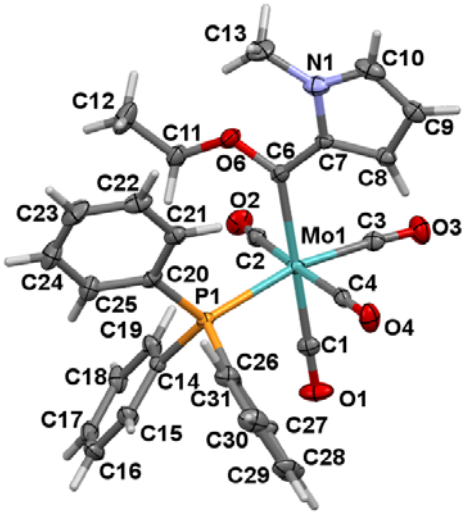

Figure 6. A perspective view of the molecular structure of **7**, showing the atom numbering scheme. Atomic displacement parameters (ADPs) are shown at the 50% probability level.

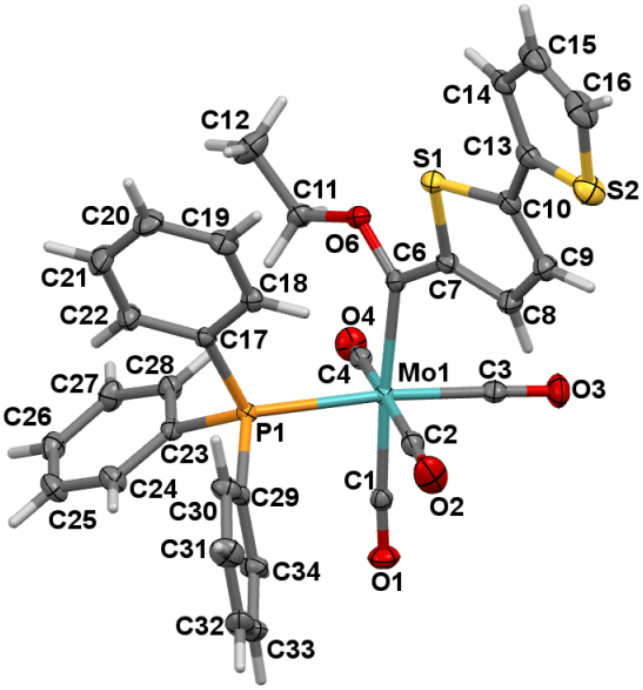

Figure 7. A perspective view of the molecular structure of **8**, showing the atom numbering scheme. Atomic displacement parameters (ADPs) are shown at the 50% probability level.

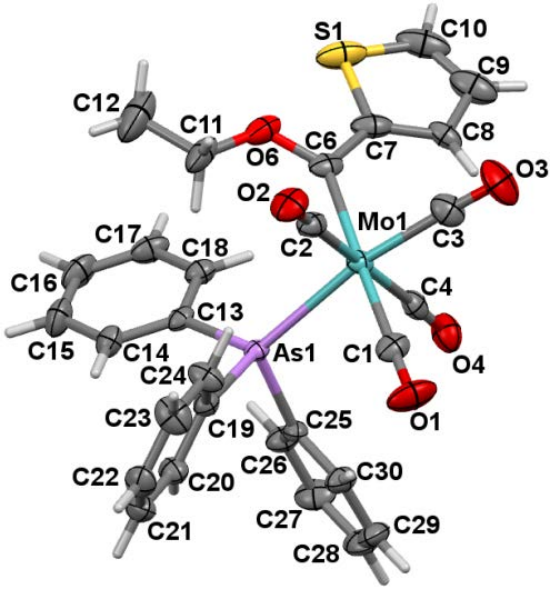

Figure 8. A perspective view of the molecular structure of **9**, showing the atom numbering scheme. Atomic displacement parameters (ADPs) are shown at the 50% probability level.

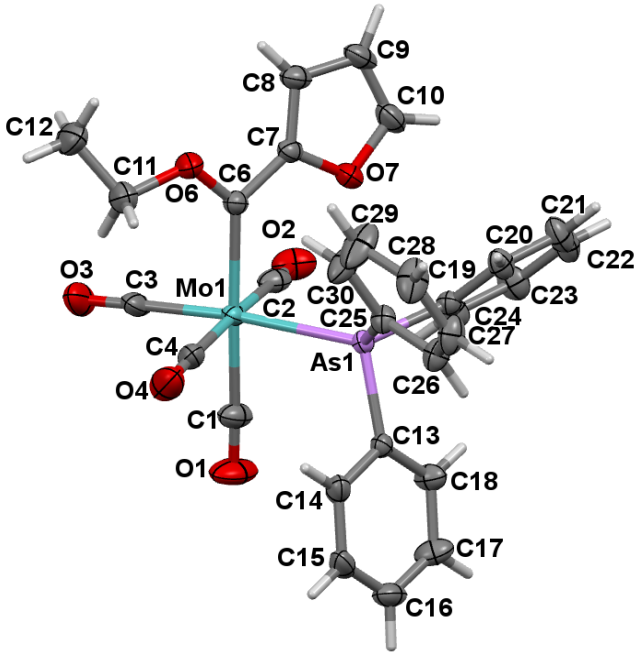

Figure 9. A perspective view of the molecular structure of **10**, showing the atom numbering scheme. Atomic displacement parameters (ADPs) are shown at the 50% probability level.

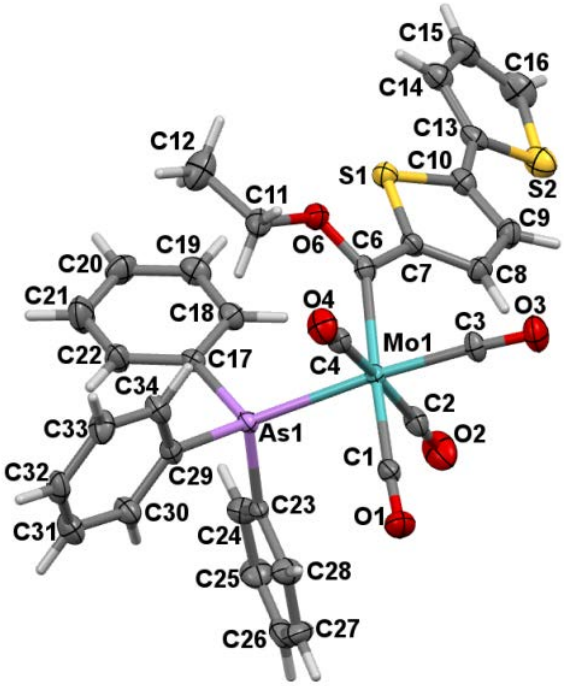

Figure 10. A perspective view of the molecular structure of **12**, showing the atom numbering scheme. Atomic displacement parameters (ADPs) are shown at the 50% probability level.

Table 1. Selected bond lengths (Å), bond angles (°), and torsion angles (°) of **1 - 4**

	1 [15,49]	**2** [13]	**3**	**4**[a]
Bond length (Å)				
Mo1-C6	2.226(5)	2.173(7)	2.225(10)	2.222(3), 2.223(3)
Mo1-C1	2.031	2.029(10)	2.033(10)	2.018(3), 2.016(3)
Mo1-C2	2.050	2.147(12)	2.04(2)	2.053(3), 2.048(3)
Mo1-C3	2.050	1.948(11)	2.050(19)	2.053(3), 2.064(3)
Mo1-C4	2.067	1.948(11)	2.050(19)	2.041(3), 2.052(3)
Mo1-C5	2.067	2.147(12)	2.04(2)	2.057(3) 2.041(3)
C6-C7	1.457(8)	1.41(4)	1.506(14)	1.456(4), 1.441(4)
C6-O6	1.333(6)	1.38(3)	1.27(2)	1.326(4), 1.329(3)
Bond angle (°)				
C6-Mo1-C5	88.29	91.6(7)	91.5(6)	93.84(10), 93.45(11)
C7-C6-Mo1	124.3(4)	130(2)	123.0(14)	124.68(18), 124.27(18)
O6-C6-Mo1	129.4(4)	127(2)	131.4(14)	129.40(18), 128.52(18)
O6-C6-C7	106.3(4)	102.6(7)	105.6(9)	105.8(2), 107.1(2)
C1-Mo1-C6	177.16	176.7(16)	178.3(12)	177.28(10), 178.01(12)
C2-Mo1-C4	176.13	175.6(3)	175.4(8)	175.16(11), 172.34(11)
C3-Mo1-C5	176.13	175.6(3)	175.4(8)	173.94(11), 178.18(11)
Torsion angle (°)				
O6-C6-C7-X[b]	0.00	180.000(4)	0.000(4)	9.2(3), -6.2(3)
C7-C8-C9-C10	0.00	0.000(5)	0.000(5)	0.6(4), -1.4(4)
Mo1-C6-C7-X[b]	-180.00	180.000(4)	180.000(4)	-166.84(13), 170.81(13)
C11-O6-C6-Mo1	0.00	0.000(4)	0.000(7)	-2.4(4), 5.5(4)
S1-C10-C13-S2	-	-	-	175.38(15), 176.24(17)

[a]Two molecules per asymmetric unit
[b]X = S1 (**1**), O7 (**2**) N1 (**3**), X = S1 (**4**)

Table 2. Selected bond lengths (Å), bond angles (°), and torsion angles (°) of **5** - **10** and **12**

	5	**6** [12]	**7**	**8**	**9**	**10**	**12**
Bond length (Å)							
Mo1-C6	2.194(3)	2.180(3)	2.245(3)	2.190(2)	2.210(2)	2.1911(19)	2.201(5)
Mo1-C1	2.003(3)	2.021(4)	1.999(3)	2.005(2)	2.019(3)	2.020(2)	2.015(6)
Mo1-C2	2.037(3)	2.036(3)	2.028(4)	2.033(2)	2.052(3)	2.041(3)	2.032(6)
Mo1-C3	1.994(3)	1.982(3)	1.975(3)	1.9796(19)	1.989(3)	1.976(2)	1.977(5)
Mo1-C4	2.038(3)	2.038(4)	2.036(4)	2.047(2)	2.053(3)	2.042(3)	2.056(6)
Mo1-E[b]	2.5667(7)	2.5626(8)	2.559(3)	2.5566(16)	2.6515(11)	2.6381(3)	2.6435(7)
C6-C7	1.452(4)	1.447(4)	1.419(4)	1.449(2)	1.449(3)	1.449(3)	1.465(8)
C6-O6	1.337(3)	1.329(4)	1.342(3)	1.333(2)	1.346(3)	1.328(3)	1.336(7)
Bond angle (°)							
C6-Mo1-E[b]	98.26(7)	94.03(7)	97.32(12)	94.73(5)	97.94(7)	92.80(5)	93.89(13)
C7-C6-Mo1	123.7(2)	124.8(1)	123.93(15)	123.44(11)	124.26(17)	124.18(15)	124.1(4)
O6-C6-Mo1	129.6(2)	131.5(2)	128.56(19)	130.41(11)	129.23(18)	131.20(14)	130.2(1)
O6-C6-C7	106.7(2)	103.6(2)	107.49(19)	106.08(14)	106.5(2)	104.48(16)	105.7(5)
C1-Mo1-C6	175.96(10)	174.55(13)	176.22(8)	176.00(6)	177.28(8)	175.35(10)	177.4(2)
C2-Mo1-C4	174.84(11)	175.60(12)	174.39(8)	172.82(6)	174.78(9)	174.74(9)	172.5(2)
C3-Mo1-E[b]	170.40(9)	173.75(9)	168.07(6)	172.77(5)	170.59(8)	174.73(6)	174.01(17)
Torsion angle (°)							
O6-C6-C7-X[c]	9.7(3)	176.1(2)	7.7(3)	17.93(17)	-7.4(2)	174.87(18)	-17.0(6)
C7-C8-C9-C10	0.4(5)	-0.1(4)	1.5(3)	1.4(2)	-1.0(4)	-0.1(3)	-2.2(8)
Mo1-C6-C7-X[c]	-173.0(2)	-7.5(4)	-173.98(15)	-159.42(8)	174.5(1)	-9.1(3)	159.8(3)
C11-O6-C6-Mo1	3.6(4)	1.0(4)	-0.1(3)	-0.4(2)	-2.9(3)	0.5(3)	1.3(7)
S1-C10-C13-S2	-	-	-	163.93(9)	-	-	-163.2(3)

[a]Two molecules per asymmetric unit
[b]E = P1 (**5**), E = P1 (**6**), E = P1 (**7**), E = P1 (**8**), E = As1 (**9**), E = As1 (**10**), E = As1 (**12**)
[c]X = S1 (**5**), X = O7 (**6**), X = N1 (**7**), X = S1 (**8**), X = S1 (**9**), X = O7 (**10**), X = S1 (**12**)

Complex **3** was refined as an inversion twin. The anisotropic displacement parameters of some atoms were restrained during the refinement to prevent them from going non-positive definite. In addition, the C6-C7 bond length was also constrained during the refinement. Complex **4** crystallized with two molecules per asymmetric unit, and both these molecules displayed orientational disorder in the position of the sulfur-atoms of the terminal thienyl-ring. The molecular structure of the main conformation for both molecules in the asymmetric unit of **4**, labeled **4a** and **4b**, have a S1-C10-C13-S2 torsion angle of approximately 180º, and that of the minor conformation approximately 0º. The ratio of the two pairs of conformations is 0.893(4):0.107(4) (**4a**:**4c**) and 0.613(4):0.387(4) (**4b**:**4c**), respectively. The main conformation of **4** is presented in **Figure 4** and shows the atomic numbering scheme used. The perspective drawings of **4b**, **4c**, and **4d** are presented in Figures S1 - S3 in the ESI.

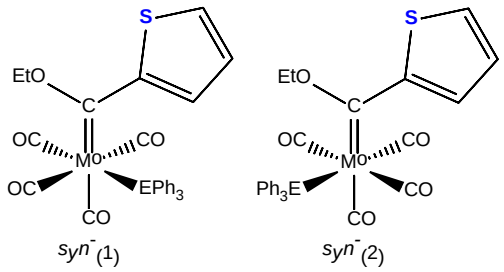

Figure 11. Two conformations of the EPh_3 ligand relative to the carbene ligand observed in the X-ray crystal structures of **5** (E = P) and **9** (E = As)

Complex **5** is disordered over two positions with the molecular structure of the major conformation (**5a**) being the *syn*-(2) conformer, as shown by the perspective view of **5** (**Figure 5**). The ratio of the *syn*-(2):*syn*-(1) isomers is 0.892(2):0.108(2) (**Figure 11**). The same scenario applies to **9**, where the ratio of the *syn*-(2):*syn*-(1) isomers is 0.795(2):0.205(2). The structures of the *syn*-(1) isomers of **5** and **9**, labelled **5b** and **9b**, are given in the ESI (Figure S4 and Figure S5). Complex **10** displayed some positional disorder for C12, and the final contribution of the two positions for C12 were determined to be in a ratio of 0.62(1):0.38(1) (**10a** and **10b**). The perspective drawing of the major conformer (**10a**) is presented in **Figure 9**, while that of **10b** is included in the ESI (Figure S6). The structure of the major conformer of **4**, **5**, **9**, and **10** is used for the discussion of the structural analyses.

It is clear from the structural information in Table 2 that Mo1-P1 and Mo1-As1 are the longest bonds in the complexes, with average lengths of 2.561(9) Å and 2.6444(8) Å, respectively. The Mo1-As1 bonds are longer than the Mo1-P1 bonds by approximately 0.1 Å.

The typical Mo1-P1 bond lengths in **5 - 8** are similar to the Mo1-P1 bond length in $[(CO)_5Mo(PPh_3)]$, which is 2.560(1) Å [50]. The Mo1-As1 bond lengths in **9**, **10**, and **12** are longer than the Mo-As bond length in $[(CO)_5Mo(AsPh_3)]$, which is reported as 2.612 Å [39]. The increased bond length in the $AsPh_3$-subsituted Fischer carbene complexes reduces steric repulsions between the sterically encumbering $AsPh_3$ and carbene ligands.

The Mo1-C6 bonds are, on average 2.214(6) Å and 2.202(3) Å for the pentacarbonyl and *cis*-tetracarbonyl complexes, respectively. The metal-carbene bond lengths are longer than the metal-carbonyl bonds. In the substituted complexes **5 - 10** and **12**, the carbonyl *trans* to another carbonyl have the longest Mo-CO bond lengths, while the carbonyl *trans* to the EPh_3 ligand have the shortest Mo-CO bond lengths. The carbonyl *trans* to the carbene ligand have intermediate Mo-CO bond lengths. These values are in agreement with the "*trans* effect" observed for $[(CO)_5M(L)]$, which states that the M-CO bond length is weakened by L in the linear fragment L-M-CO according to: L = CO > PR_3 > AsR_3 [47]. In the current examples, the Mo(0) complexes showed no significant variation for the M-CO bond length for the carbonyl *trans* to PPh_3 and $AsPh_3$. The Mo-C3 bond lengths in **5**, **6**, and **8** are similar to those in **9**, **10**, and **12**, respectively**.** The C-O bond lengths of the carbonyl ligands showed no trend, similar to what was observed for C-O bond lengths of $[(CO)_5M(EPh_3)]$ with M = Cr, Mo, W and E = P, As, Sb [39], as well as for *cis*-$[(AsPh_3)_2(CO)_4M]$ with M = Mo, W [51]. Cotton and Wing argued that alterations to the C-O bond orders do not influence the C-O bond lengths to an observable degree [52]. In the pentacarbonyl complexes, the C6-O6 bond length for **3** is shorter by roughly 0.1 Å than the C6-O6 bonds in **1** [12], **2** [15], and **4**. Furthermore, the C6-C7 bond length for **3** is longer by an estimate 0.1 Å than the corresponding bond in **1** [12], **2** [15], and **4**. These trends were not observed for the *cis*-substituted tetracarbonyl complexes (**5 - 12**) [12].

The C1-Mo1-C6, C2-Mo1-C4, and C3-Mo1-E bond angles for all the substituted complexes deviate from the ideal value of 180° for octahedral complexes. This is due to the steric stress introduced by the *cis*-orientation of the carbene and EPh_3 ligands. Less deviation from 180° is observed for **1 - 4** [13,15,49], which lack the bulky EPh_3 ligand. A sp^2-hybridization is expected for the carbene carbon, thus bond angles around it should have an ideal value of 120°. The bond angles C7-C6-Mo1, O6-C6-Mo1, and O6-C6-C7 deviate from the ideal value. This is due to the presence of the bulky metal moiety. The C7-C6-Mo1 and O6-C6-Mo1 bond

angles are all larger than 120°, while the O6-C6-C7 bond angles are approximately 15° smaller than the ideal value [12-15,40,49].

The O6-C6-C7-X torsion angle is an indication of the orientation of the ethoxy and heteroaryl carbene substituents. Torsion angle values close to 0° indicates a *syn* orientation [53] of the two substituents while values in the region of 180° indicate an *anti* orientation (ethoxy O-atom and heteroarene heteroatom facing in opposite directions). All of the 2-thienyl, 2-(N-methyl)pyrrolyl, and 2-2'-bithienyl complexes are *syn*, with torsion angle values that deviate from the ideal value of 0° by 17.93(17)° or less [13,15,49]. The 2-furyl complexes, **2** [13], **6** [12], and **10**, have *anti* orientations, with an average O6-C6-C7-O7 torsion angle of 176.9(6)°. The C7-C8-C9-C10 torsion angles for all the complexes of the study indicate planarity of the heteroaryl ring, with values that are close to 0° [12,13,15]. The two thienyl rings of the 2,2'-bithienyl moiety of **4** are in a planar conformation, with S1-C10-C13-S2 torsion angles of 175.38(15)° and 176.24(17)° for the two molecules of **4** in the asymmetric unit. The planarity of the 2,2'-bithienyl moiety is lifted upon carbonyl substitution, as these torsion angles in **8** and **12** are 163.93(9)° and 163.2(3)°, respectively. The loss of planarity results in a disruption of the conjugation of the two thienyl rings and the carbene carbon.

Orbital overlap between the carbene carbon and its substituents is required to allow for effective electron density donation [54]. The C11-O6-C6-Mo1 torsion angles have values ranging from 0° to 5.5°, indicating good planarity of the ethoxy group with the metal-carbene bond. The monomeric heteroarenes deviate from planarity with the C6-Mo1 bond by angles ranging from 0° to 10°, as indicated by the Mo1-C6-C7-X torsion angles having values close to 0° or 180°. The 2,2'-bithienyl substituents deviate from planarity with the metal-carbene bond roughly 20° for **8** and **12**, and by ±13° for **4**.

3.4 DFT study

Various conformations and isomers are possible for each of complexes **1** - **12**. For example, the heteroaryl group can be orientated *syn* or *anti* relative to the ethoxy group and the pnictogen ligands can be positioned *cis* or *trans* relative to the carbene ligand. Furthermore, two conformations are possible for each of the *cis* isomers of complexes **5** - **12**, as illustrated in Figure 11, and indeed observed in the crystal structures of **5** and **9**. The density functional theory (DFT) calculated gas phase electronic energies of the *cis*- and *trans* isomers for the different conformers and isomers are given in

Table **3**. The results, in agreement with experimental findings, indicate that:

(i) The *cis*-isomers for all eight tetracarbonyl complexes (**5 - 12**) are more stable than the corresponding *trans*-isomers.
(ii) Conformers with the aryl group *syn* to the ethoxygroup for Ar = 2-thienyl, 2-(N-methyl)pyrrolyl or 2,2'-bithienyl and *anti* to the ethoxygroup for Ar = 2-furyl, have the lowest energy.
(iii) The *cis* isomers of the tetracarbonyl complexes (**5 - 12**), with the PPh_3 or $AsPh_3$ group in position (1) or (2) (Figure 11) are equi-energetic.
(iv) Conformers of the complexes **8** and **12** with a *syn-anti* and *syn-syn* orientation of the 2,2'-bithienyl moiety are equi-energetic.

The *anti*-orientation of the 2-furyl ring in **2** [13], **6** [12] and **10** contrasts the *syn*-orientation of the 2-thienyl, 2-(N-methyl)pyrrolyl, and 2,2'-bithienyl moieties. This is due to the interaction between the lone pair of electrons on the oxygen of the 2-furyl ring and anti-bonding orbitals on the adjacent carbonyl group(s). An NBO analysis of complexes **2**, **6** and **10** showed conjugative interactions between a lone pair present on the 2-furyl O-atom (LP) and the antibonding orbital present in a carbonyl ligand (BD*). Figure 12 visualize the LP(O) → BD*(C-O) interactions, and the second order perturbation theory interaction energies are given in Table 4.

The *syn*-orientation of the 2-(N-methyl)pyrrolyl group in complexes **3**, **7** and **11** is due to the interaction between the lone pair of electrons on the oxygen of the ethoxy group and an anti-bonding orbital present on the methyl group of the 2-(N-methyl)pyrrolyl functionality. The LP(O) → BD*(C-H) natural bonding orbital (NBO) interaction, as obtained from an NBO analysis of the complexes, is visualized in **Figure 13**, and the second order perturbation theory interaction energies are given in **Table 4**.

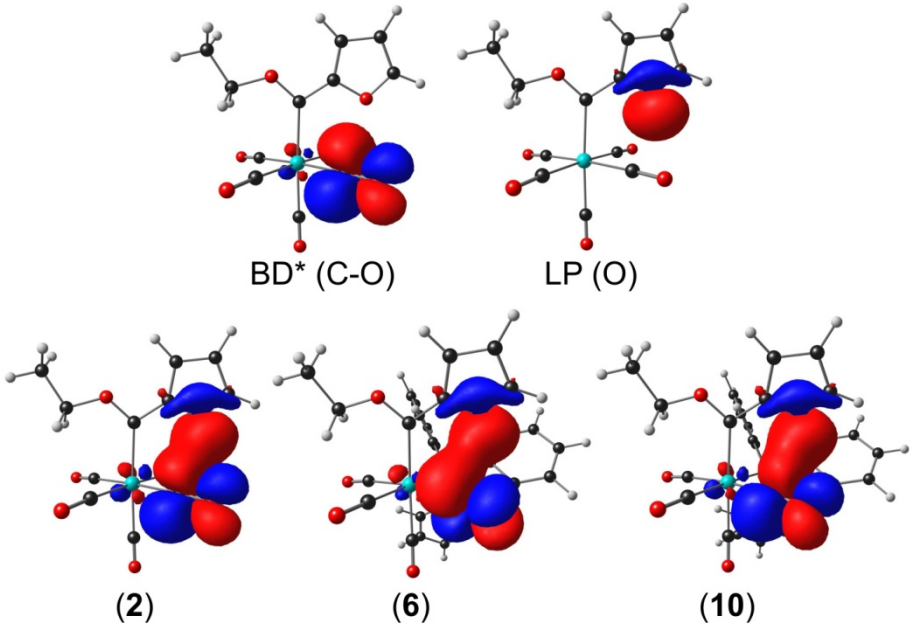

Figure 12. Bottom: LP(O) → BD*(C-O) interactions present in the 2-furyl complexes **2**, **6** and **10**. Top: The NBOs of **2** involved in the LP(O) → BD*(C-O) interaction for **2**.

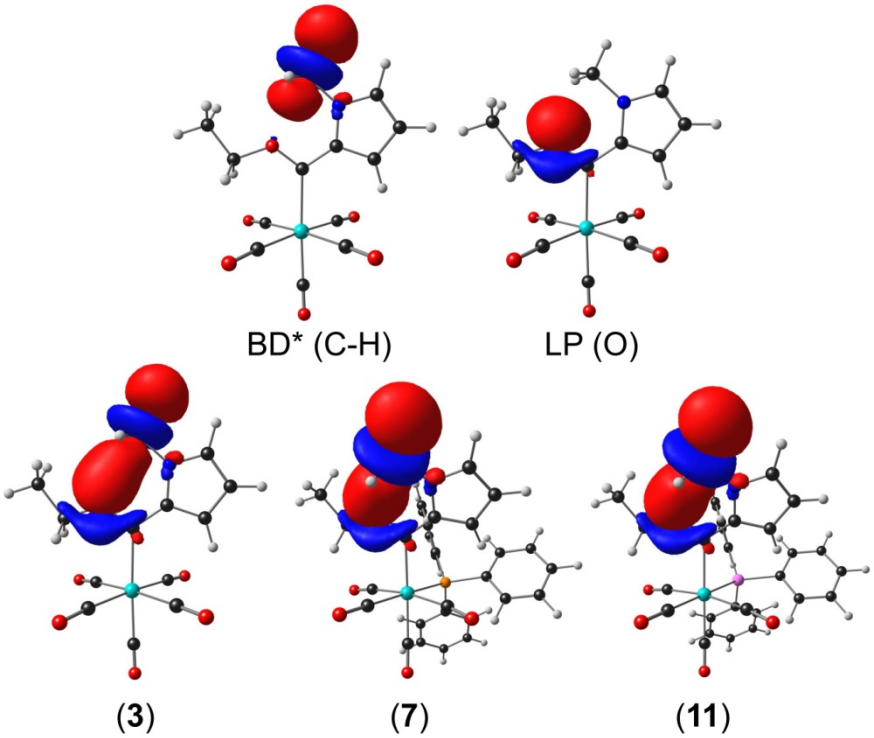

Figure 13. Bottom: LP(O) → BD*(C-H) interactions present in the 2-furyl complexes **3**, **7** and **11**. Top: The NBOs of **3** involved in the LP(O) → BD*(C-H) interaction for **3**.

Table 3. Relative energies of the optimized conformers and isomers of complexes **1** - **12**. The energy of the lowest energy conformers of each complex is highlighted in bold.[a]

	1	**2**	**3**	**4**		
anti	0.11	**0.00**	0.24	-		
syn	**0.00**	0.08	**0.00**	-		
anti-anti	-	-	-	0.14		
anti-syn	-	-	-	0.11		
syn-anti	-	-	-	**0.00**		
	5	**6**	**7**	**9**	**10**	**11**
cis-anti (1)	0.15	**0.00**	0.24	0.14	**0.00**	0.24
cis-anti (2)	0.12	**0.01**	0.25	0.12	**0.02**	0.25
cis-syn (1)	**0.00**	0.08	**0.00**	**0.00**	0.09	**0.00**
cis-syn (2)	**0.01**	0.08	**0.04**	**0.01**	0.09	**0.04**
trans-anti	0.20	0.08	0.35	0.21	0.09	0.35
trans-syn	0.10	0.18	0.14	0.10	0.18	0.14
		8			**12**	
cis-anti-anti (1)		0.20			0.19	
cis-anti-anti (2)		0.16			0.16	
cis-anti-syn (1)		0.16			0.14	
cis-anti-syn (2)		0.13			0.13	
cis-syn-anti (1)		**0.00**			**0.00**	
cis-syn-anti (2)		**0.02**			**0.02**	
cis-syn-syn (1)		**0.03**			**0.03**	
cis-syn-syn (2)		**0.04**			**0.04**	
trans-anti-anti		0.24			0.24	
trans-anti-syn		0.21			0.21	
trans-syn-anti		0.11			0.11	
trans-syn-syn		0.14			0.03	

[a] *Syn* and *anti* refer to the position of the aryl group(s) relative to the ethoxy group, *cis* and *trans* refer to the position of the EPh_3 ligand relative to the carbene ligand in **5** - **12**, (1) and (2) are defined in **Figure 11**.

Table 4. Second order perturbation theory interaction energies, E(2), and NBO occupations calculated for the indicated complexes

Complex	**2**	**6**	**10**	**3**	**7**	**11**
E(2) / kJ·mol^{-1}	< 2[a]	4.18	3.97	4.85	3.81	4.02
Occupancy LP/ e	1.964	1.962	1.962	1.960	1.961	1.961
Occupancy BD* / e	0.135	0.152	0.148	0.008	0.008	0.008

[a] Interaction observed from evaluation of NBOs, but threshold for printing of NBO program is 2 kJ·mol^{-1}

4 Conclusions

X-ray crystal structures of molybdenum(0) Fischer carbene complexes containing a heteroaryl substituent on the carbene ligand showed that intramolecular communication between the carbene ligand, the metal centre, and the ancillary ligands is possible due to the planarity of the carbene substituents and the metal-carbene bond. Enhanced donor-acceptor properties of PPh_3 over $AsPh_3$ were established by ^{13}C-NMR data, while no such conclusion could be drawn from the metal-carbonyl bond lengths nor the IR spectral data. The geometry of the DFT calculated lowest energy isomers or conformers were in agreement with the experimental crystal structures. An NBO analysis of selected complexes showed lone-pair →

anti-bonding orbital interactions leading to *syn* and *anti* orientations of the 2-(N-methyl)pyrrolyl and 2-furyl groups relative to the ethoxy group, respectively.

Disclosure statement

The authors declare no conflict of interest.

Funding

This work has received support from the Norwegian Supercomputing Program (NOTUR) through a grant of computer time (Grant No. NN4654K) (JC), the South African National Research Foundation (JC, ML) and the Central Research Fund of the University of the Free State, Bloemfontein (JC) and the University of Pretoria (ML).

References

[1] E.O. Fischer, A. Maasböl, Chem. Ber. **100** (1967) 2445-2456

[2] E.O. Fischer, G. Kreis, C.G. Kreiter, J. Müller, G. Huttner, H. Lorenz, Angew. Chem. Int. Ed. **12** (1973) 546-565.

[3] C.P. Casey, M.C. Cesa, Organometallics **1** (1982) 87-94.

[4] E.O. Fischer, R. Aumann, Chem. Ber. **102** (1969) 1495-1503.

[5] E.O. Fischer, H. Fischer, Chem. Ber. **107** (1974) 657-672.

[6] E.O. Fischer, K. Richter, Chem. Ber. **109** (1976) 1140-1157.

[7] K.H. Dötz, H. Larbig, K. Harms, Chem. Ber. **125** (1992) 2143-2148.

[8] J. Barluenga, K. Muñiz, M. Tomás, A. Ballesteros, S. García-Granda, Organometallics **22** (2003) 1756-1760.

[9] K.H. Dötz, Angew. Chem. Int. Ed. **23** (1984) 587-608.

[10] J. Barluenga, M.A. Fernández-Rodríguez, E. Aguilar, J. Organomet. Chem. **690** (2005) 539-587.

[11] K.H. Dötz, J. Stendel Jr., Chem. Rev. **109** (2009) 3227-3274.

[12] M. Landman, T. Levell, P.H. van Rooyen, J. Conradie, J. Mol. Struct. **1065-1066** (2014) 29-38.

[13] M. Landman, T.J. Levell, M.M. Conradie, P.H. van Rooyen, J. Conradie, J. Mol. Struct. **1086** (2015) 190-200.

[14] A. Jansen van Rensburg, M. Landman, P.H. van Rooyen, M.M. Conradie, J. Conradie, J. Mol. Struct. **1105** (2016) 205-213

[15] M. Landman, H. Görls, S. Lotz, Z. Anorg. Allg. Chem. **628** (2002) 2037-2043.

[16] G.H. Spies, R.J. Angelici, Organometallics **6** (1987) 1897-1903.

[17] W.L.F. Armarego, D.D. Perrin, Purification of laboratory chemicals (1996) Reed Educational and Professional Publishing Ltd., Oxford.

[18] H. Meerwein, Org. Synth. **46** (1966) 113.

[19] APEX2 (including SAINT and SADABS), Bruker AXS Inc., Madison, WI (2012).

[20] G.M. Sheldrick, Acta Crystallogr. Sect. A: Found. Crystallogr. **64** (2008) 112-122.

[21] L.G. Farrugia, J. Appl. Crystallogr. **30** (1997) 565-566.

[22] A.D. Becke, Phys. Rev. A **38** (1988) 3098-3100.

[23] C.T. Lee, W.T. Yang, R.G. Parr, Phys. Rev. B **37** (1988), 785-789.

[24] J. Stephens, F.J. Devlin, C.F. Chabalowski, M.J. Frisch, J. Phys. Chem. **98** (1994), 11623-11627.

[25] M.J. Frisch, G.W. Trucks, H.B. Schlegel, G.E. Scuseria, M.A. Robb, J.R. Cheeseman, G. Scalmani, V. Barone, B. Mennucci, G.A. Petersson, H. Nakatsuji, M. Caricato, X. Li, H.P. Hratchian, A.F. Izmaylov, J. Bloino, G. Zheng, J.L. Sonnenberg, M. Hada, M. Ehara, K. Toyota, R. Fukuda, J. Hasegawa, M. Ishida, T. Nakajima, Y. Honda, O. Kitao, H. Nakai, T. Vreven, J.A. Montgomery (Jr), J.E. Peralta, F. Ogliaro, M. Bearpark, J.J. Heyd, E. Brothers, K.N. Kudin, V.N. Staroverov, T. Keith, R. Kobayashi, J. Normand, K. Raghavachari, A. Rendell, J.C. Burant, S.S. Iyengar, J. Tomasi, M. Cossi, N. Rega, J.M. Millam, M. Klene, J.E. Knox, J.B. Cross, V. Bakken, C. Adamo, J. Jaramillo, R. Gomperts, R.E. Stratmann, O. Yazyev, A.J. Austin, R. Cammi, C. Pomelli, J.W. Ochterski, R.L. Martin, K. Morokuma, V.G. Zakrzewski, G.A. Voth, P. Salvador, J.J. Dannenberg, S. Dapprich, A.D. Daniels, O. Farkas, J.B. Foresman, J.V. Ortiz, J. Cioslowski, D.J. Fox, Gaussian 09, Revision B.01, Gaussian, Inc., Wallingford, CT, 2013.

[26] F. Weigend, R. Ahlrichs, Phys. Chem. Chem. Phys. **7** (2005), 3297-3305.

[27] J.P. Foster and F. Weinhold, J. Am. Chem. Soc. **102** (1980) 7211-7218.

[28] A.E. Reed, F. Weinhold, J. Phys. Chem. **83** (1985) 1736-1740.

[29] A.E. Reed, R.B. Weinstock, F. Weinhold, J. Chem. Phys. **83** (1985) 735-746.

[30] A.E. Reed, L.A. Curtiss, F. Weinhold, Chem. Rev. **88** (1988) 899-926.

[31] NBO 3.1. E.D. Glendening, J.K., Badenhoop, A.E., Reed, J.E., Carpenter, J.A., Bohmann, C.M., Morales, F. Weinhold (Theoretical Chemistry Institute, University of Wisconsin, Madison, WI, 2001).

[32] M. Landman, R. Fraser, L. Twigge, J. Conradie, J. Coord. Chem. **68** (2015) 2388-2408.

[33] M Landman, J. Conradie, J. Mol. Struct., **1094** (2015) 36-45.

[34] M. Landman, B.E. Buitendach, M.M. Conradie, R. Fraser, P.H. van Rooyen, J. Conradie, **739** (2015) 202–210.

[35] E.O. Fischer, Angew. Chem. **86** (1974) 651-663.

[36] E.O. Fischer, Pure Appl. Chem. **30** (1972) 353-372.

[37] H. Werner, H. Rascher, Inorg. Chim. Acta **2** (1968) 181-185.

[38] C.N. Matthews, T.A. Magee, J.H. Wotiz, J. Am. Chem. Soc. **81** (1959) 2273-2274.

[39] M.J. Aroney, I.E. Buys, M.S. Davies, T.W. Hambley, J. Chem. Soc. Dalton Trans. (1994) 2827-2834.

[40] M. Landman, R. Pretorius, R. Fraser, B.E. Buitendach, M.M. Conradie, P.H. van Rooyen, J. Conradie, Electrochim. Acta **130** (2014) 104-118.

[41] E.O. Fischer, H. Fischer, H. Werner, Angew. Chem. Int. Ed. **11** (1972) 644-645.

[42] A. Arietta, F.P. Cossío, I. Fernández, M. Gómez-Gallego, B. Lecea, M.J. Mancheño, and M.A. Sierra, J. Am. Chem. Soc. **122** (2000) 11509-11510.

[43] H. Werner, Angew. Chem. Int. Ed. **7** (1968) 930-941.

[44] L. Lancelotti, R. Tubino, S. Luzzati, E. Licandro, S. Maiorana, A. Papagni, Synth Met. **93** (1998) 27-32.

[45] P.S. Braterman, D.W. Milne, E.W. Randall, E. Rosenberg, J. Chem. Soc., Dalton Trans. (1973) 1027-1031.

[46] W.A. Schenk, W. Buchner, Inorg. Chim. Acta **70** (1983) 189-196.

[47] W. Buchner, W.A. Schenk, Inorg. Chem. **23** (1984) 132-137.

[48] E.W. Abel, M.A. Bennett, G. Wilkinson, *J. Chem. Soc.* (1959), 2323-2327.

[49] Cambridge Structural Database (CSD), version 5.37, 2016, CSD reference code: WUCRIV.

[50] F.A. Cotton, D.J. Darensbourg, H.W. Ilsley, Inorg. Chem. **20** (1981) 578-583.

[51] C.L. Bergstrom, R.L. Luck, Inorg. Chim. Acta **318** (2001), 77-83.

[52] F.A. Cotton and R.M. Wing, Inorg. Chem. **4** (1965) 314-317.

[53] S. Thompson, H.R. Wessels, R. Fraser, P.H. van Rooyen, D.C. Liles, M. Landman, J. Mol. Struct. **1060** (2014), 111-118.

[54] U. Schubert, Coord. Chem. Rev. **55** (1984), 261-286.